J. Fluid Mech. (2010), *vol.* 657, *pp.* 1–21.
doi:10.1017/S002211201000128X

Wall effects on a rotating sphere

QIANLONG LIU[1] AND ANDREA PROSPERETTI[1,2]†

[1]Department of Mechanical Engineering, Johns Hopkins University, Baltimore, MD 21218, USA

[2]Faculty of Science and Technology and J. M. Burgers Centre for Fluid Dynamics, University of Twente, P.O. Box 217, 7500 AE Enschede, The Netherlands

(Received 26 September 2009; revised 26 January 2010; accepted 9 March 2010; first published online 26 May 2010)

The flow induced by a spherical particle spinning in the presence of no-slip planar boundaries is studied by numerical means. In addition to the reference case of an infinite fluid, the situations considered include a sphere rotating near one or two infinite plane walls parallel or perpendicular to the axis of rotation and a sphere centred within a cube. The hydrodynamic force and couple acting on the sphere exhibit a complex behaviour under the sometimes competing, sometimes cooperating action of viscous, inertial and centrifugal effects.

1. Introduction

At a very low Reynolds number, a couple-free spherical particle suspended in a viscous fluid rotates with the local angular velocity of the fluid (see e.g. Happel & Brenner 1973; Kim & Karrila 1991). However, a non-negligible moment of inertia will cause a transient rotation relative to the surrounding fluid. For example, in a fluidized bed, particles acquire angular momentum under the effect of collisions or by traversing a vortical region, and they may retain this angular momentum as they move to a different region (see e.g. Wu *et al.* 2008*a*,*b*). The process that forms fuel drops in a spray may impart to them an initial angular velocity (see e.g. Xin & Megaridis 1996). A heavy particle may settle out of a rotating fluid mass. The hydrodynamic force and couple acting on the particle in these and other instances are modified by the presence of nearby boundaries, with consequences on spin-up and spin-down time, wall deposition, entrainment and others. Furthermore, particle rotation acts as a source of angular momentum for a fluid, just as drag and lift act as sources of linear momentum, and may need to be included in an averaged-equation model of disperse systems.

Recent advances in microfluidics, where the proximity of boundaries is all but unavoidable, are another reason of interest in these phenomena. For example, Leach *et al.* (2009) have measured the angular velocity of a microsphere held in place near a boundary by optical tweezers. The rotating sphere viscometer is based on the relation between the applied couple and the resulting angular velocity (see e.g. Walters & Waters 1963, 1964; Besseris, Miller & Yeates 1999; Parkin *et al.* 2007). This principle has recently been used to measure the viscosity of minute liquid samples and intracellular fluids by means of rotating microspheres (Besseris *et al.* 1999; Parkin *et al.* 2007).

† Email address for correspondence: prosperetti@jhu.edu

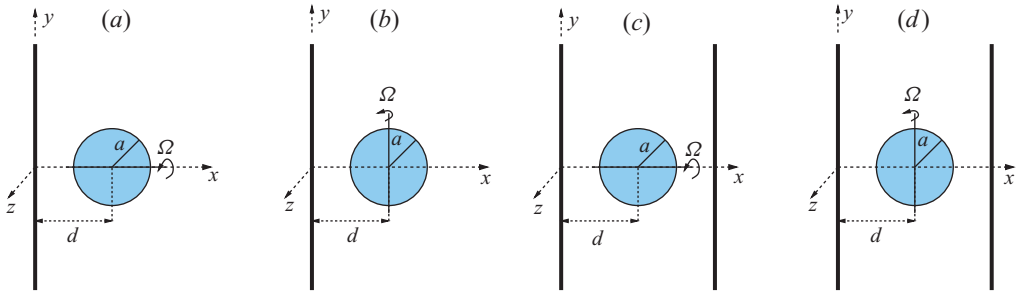

FIGURE 1. (Colour online) Four of the situations studied in this paper; the thick lines denote solid boundaries, to which the rotation axis is perpendicular in (a,c) (§§ 4 and 6) and parallel in (b,d) (§§ 5 and 6).

The rotation of a sphere in a quiescent viscous fluid, with and without inertia, has been the object of several papers. Banks (1976) has studied the flow and the hydrodynamic couple on a steadily rotating sphere with a fixed centre in the boundary-layer approximation, while Dennis and co-workers (Dennis, Singh & Ingham 1980; Dennis, Ingham & Singh 1981) have solved the full Navier–Stokes problem. The boundary layer on a sphere impulsively set into rotation has been studied by Barrett (1967), while the complete time-dependent problem has been solved by Dennis & Duck (1988) and the Stokes-flow version by Feuillebois & Lasek (1978). Hollerbach *et al.* (2002) have studied the flow caused by the torsional oscillations of a sphere in a fluid at rest.

The effect of boundaries, however, has only been considered in the low-Reynolds-number regime, starting with the theoretical papers of Jeffery (1915), Dean & O'Neill (1963) (corrected in Goldman, Cox & Brenner 1967), O'Neill (1964), Cox & Brenner (1967*a*), Cox & Brenner (1967*b*), Takagi (1974) and Chaoui & Feuillebois (2003). The study of Malysa & van de Ven (1986) has provided experimental confirmation of some of these results. The studies of Ganatos, Pfeffer & Weinbaum (1980*a*) and Ganatos, Weinbaum & Pfeffer (1980*b*) on the slow motion of a sphere between two parallel walls have been extended to droplets by Keh & Chen (2001), and contain some limited results on the effects of rotation. Recent work, motivated by an interest in the interaction of cells or microspheres with the glycocalix, has considered the translational and rotational motion of a sphere near a Brinkman medium (Damiano *et al.* 2004), again with the neglect of inertial effects.

The purpose of the present paper is to investigate inertial effects on the hydrodynamic interaction of a spinning sphere of radius a at a distance d from one or more boundaries. The centre of the sphere is taken to be fixed. We consider spheres rotating about axes parallel or perpendicular to a single no-slip plane or between two parallel planes (figure 1). The results depend on the two dimensionless parameters

$$\frac{d}{a} \qquad \text{and} \qquad Re = \frac{a^2\Omega}{\nu} \tag{1.1}$$

in which Ω is the angular velocity of the sphere and ν is the kinematic viscosity of the fluid.

The situation considered here is simpler than the one in which the fluid rotates, or the sphere translates in addition to rotating. There are many papers dealing with these more complex situations. A good review is provided by Bush, Stone & Tanzosh (1994). Among the more recent contributions, we may mention the studies by Minkov,

Ungarish & Israeli (2000) and Minkov, Ungarish & Israeli (2002) on the translation of particles in finite-size containers and the study of Loper (2001) on the structure of the Taylor columns that form in these conditions.

Similarly to the case of rotating disks and cones, with increasing Reynolds number the flow induced by a sphere rotating in an unbounded fluid becomes unstable as studied experimentally and theoretically by several investigators (see e.g. Kohama & Kobayashi 1983; Wimmer 1988; Taniguchi, Kobayashi & Fukunishi 1998; Garrett & Peake 2002). The Reynolds number at which these phenomena take place is larger than the ones considered in this paper.

2. Numerical method

We use the combined immersed-boundary, finite-difference PHYSALIS method to solve the Navier–Stokes equations for an incompressible, constant-property Newtonian fluid. The method is described in detail elsewhere (Zhang & Prosperetti 2005) and a very brief description will be sufficient here.

Because of the no-slip condition, near the particle the fluid-particle relative velocity is very small. In the rest frame of the particle, therefore, the Navier–Stokes equations can be linearized to the Stokes form. The exact solution of these equations can be expressed analytically as an infinite series containing undetermined coefficients (see e.g. Lamb 1932; Kim & Karrila 1991). Farther away from the particle surface (in practice, at distances of the order of one mesh length), the nonlinear terms become important and the solution is calculated by an explicit standard projection method with first-order accuracy in time and second-order accuracy in space.

An iterative process brings the finite-difference and the analytic solution in agreement by the following procedure: (i) the current finite-difference solution for pressure and vorticity is used to estimate the undetermined coefficients after a suitable truncation of the infinite series; (ii) this estimate is used to set velocity boundary conditions at the grid points adjacent to the particle surface; (iii) a new finite-difference solution satisfying these boundary conditions is calculated, and the process repeated to convergence. Noteworthy features of the method are the following:

(*a*) The no-slip condition at the particle surface is satisfied exactly;

(*b*) The lower-order undetermined coefficients give the force and torque on the sphere directly, thus avoiding the need to integrate the numerically calculated fluid stress over the particle surface;

(*c*) If the Stokes approximation is used beyond its approximate domain of validity, our experience is that the iterative process will not converge. In this respect, the method contains a built-in accuracy test.

We apply the no-slip condition on the other solid boundaries. Different conditions are appropriate on the remaining boundaries of the computational domain depending on the problem. In an unbounded fluid, or when the axis of rotation is parallel to the plane wall(s), there is symmetry about a plane through the sphere centre and normal to the axis and corresponding conditions are imposed on the boundaries parallel to this plane on both velocity and pressure. On the other boundaries and in the other cases we have tried both periodicity conditions and zero gradients normal to the boundary. The differences on the computed couples and forces were small, of the order of 1 %. The streamline pattern was essentially identical near the particle and visibly affected only near the boundaries. The results shown are for zero-normal-gradient conditions.

Because of its reliance on the existence of a thin Stokes-like region near the sphere surface, the simulation of large-Reynolds-number flows requires a very fine

	$Re=2$	$Re=10$	$Re=20$	$Re=50$	$Re=100$
Dennis *et al.* (1980)	1.0034	1.0741	1.2128	1.5458	1.9218
Present work	1.0038	1.0692	1.1980	1.5207	1.8781

TABLE 1. Comparison of the present results for the normalized hydrodynamic torque $-L/8\pi\mu\Omega a^3$ acting on a sphere rotating in an unbounded fluid with the results given by Dennis *et al.* (1980) for different Reynolds numbers, $Re=a^2\Omega/\nu$.

grid which limits the total size of the computational domain. In this work, this constraint is alleviated somewhat by placing the particle at the centre of a cubic region discretized with twice as many grid points in each direction as the rest of the computational domain. Herein lies the main difference between the code used for the present computations and that described by Zhang & Prosperetti (2005). In spite of this refinement, in order to have simulation times sufficiently short to permit a parametric study, we have been forced to limit ourselves to a maximum Reynolds number of the order of 100 and therefore smaller than that used by some earlier investigators. In particular, Dennis *et al.* (1980, 1981) and Dennis & Duck (1988) were able to consider values of Re of the order of 10^3 by using a method specifically designed for a sphere in an unbounded fluid. That method, however, could not be used to explore the effect of boundaries, which is the main thrust of the present study.

The size of the domain necessary to obtain a solution essentially unaffected by the computational boundaries decreases with increasing Reynolds number while the mesh length necessary for grid independence has the opposite trend. Suitable values for these parameters were determined by trial and error. For the cases of §§ 3 (unbounded fluid) and 4 (one wall, perpendicular axis), the computational domain was a cube with a side of between 10 and 17 particle radii discretized with 50–60 cells; between 3 and 6 coarse cells per particle radius were used, increasing with the Reynolds number. Because of the use of the refined grid, the actual number of cells used near the particle was actually double. For the simulations of § 5 (one wall, parallel axis) the computational domain was a parallelepiped elongated in the directions parallel to the wall with sides of 11–16 radii (about 50 cells) normal to the wall, 10–20 radii (50–60 cells) in the direction of the axis and 16–26 radii (80–90 cells) in the third direction. There were between 3 and 6 coarse cells per radius. For the two-wall cases of § 6, the computational domain extended 8–12.5 radii (50 cells) in the directions parallel to the walls and between 4 and 6 coarse cells per radius were used. For the closed enclosure case of § 7 we used between 4 and 9 coarse cells per particle radius. The side of the fine-grid cube surrounding the particle was between 3 and 6 radii. Most of the computations were repeated with different grids to make sure that the results shown are essentially grid independent.

For all the simulations the calculation was started from rest by impulsively imposing the required angular velocity on the sphere. The calculation was continued until a steady state was reached as indicated by the time independence of forces and couples. The explicit time integration puts a stringent upper bound on the time step. The simulations were conducted with a step adjusted as recommended by Peyret & Taylor (1983, p. 148) and Fletcher (1988, vol. 2, p. 335).

In table 1 we compare the torque on a sphere spinning in an infinite fluid as calculated by Dennis *et al.* (1980) with those given by the present method. The two sets of results are within 1–2 %. Table 2 shows the effect of different domain size

H/a	$a/\Delta x$	$-L/8\pi\mu\Omega a^3$
10.4	10	1.519
7.2	10	1.515
5.6	10	1.494
11.1	9	1.512

TABLE 2. Normalized hydrodynamic torque $-L/8\pi\mu\Omega a^3$ acting on a sphere rotating in an unbounded fluid as computed with domains of different sizes and different mesh lengths Δx. The computational domain is a cube of side H centred at the sphere centre. The Reynolds number is 50.

d/a	Exact, Stokes flow	Present, $Re = 10^{-3}$
1.5	1.0391	1.0396
1.75	1.0241	1.0235
2	1.0159	1.0153
3	1.0047	1.0040

TABLE 3. Normalized hydrodynamic torque $-L/8\pi\mu\Omega a^3$ acting on a sphere centred at a distance d from a plane and rotating around an axis normal to the wall as given by the Stokes-flow solution of Jeffery (1915) and the present method. The present results for $Re = 10^{-2}$ are identical to those shown.

and mesh lengths for a sphere in an unbounded fluid for $Re = 50$, and table 3 is a comparison of the present results for $Re = 10^{-3}$ and 10^{-2} with the analytic solution of Jeffery (1915) for the near-wall situation of figure 1(*b*). All these comparisons demonstrate the satisfactory accuracy of the present computations.

3. Rotation in an unbounded fluid

The case of a sphere rotating in an unbounded fluid is useful both to test of the accuracy of the simulations and to gain insight into some basic physical aspects of the situation. The sphere rotates with a positive angular velocity around the z-axis.

3.1. *The steady-state problem*

The hydrodynamic couple $\boldsymbol{L}$ on the sphere is given by

$$\boldsymbol{L} = \oint \boldsymbol{x} \times (\boldsymbol{\tau} \cdot \boldsymbol{n}) \, \mathrm{d}S \tag{3.1}$$

where the integral is over the sphere surface, $\boldsymbol{x}$ is the position vector with respect to the sphere centre of the surface element $\mathrm{d}S$ on which the unit outward normal is $\boldsymbol{n}$ and $\boldsymbol{\tau}$ is the viscous stress tensor. The only non-zero component of $\boldsymbol{L}$ is along the axis of rotation $\boldsymbol{\Omega}/|\boldsymbol{\Omega}|$ and is given by

$$L \equiv \frac{\boldsymbol{\Omega}}{|\boldsymbol{\Omega}|} \cdot \boldsymbol{L} = 2\pi a^3 \int_0^\pi \sin^2\theta \, \tau_{r\phi} \, \mathrm{d}(\cos\theta) \simeq \frac{8}{3}\pi a^3 \tau_{r\phi}, \tag{3.2}$$

in which $\tau_{r\phi}$ is a component of the viscous stress tensor and (r, θ, ϕ) refer to a spherical coordinate system with the polar axis along the axis of rotation. At a high Reynolds number, we may use the estimate

$$\tau_{r\phi} \simeq \frac{\mu}{2} \frac{-\Omega a}{\sqrt{\nu/\Omega}} \tag{3.3}$$

to find

$$-\frac{L}{(\pi\rho a^5\Omega^2)/2} \simeq \frac{8}{3}Re^{-1/2}. \tag{3.4}$$

A more detailed calculation in the boundary-layer approximation (Banks 1976) gives a somewhat different value of the numerical coefficient, namely

$$-\frac{L}{(\pi\rho a^5\Omega^2)/2} \simeq 2.06\,Re^{-1/2} \tag{3.5}$$

which has been confirmed by the full Navier–Stokes simulations of Dennis *et al.* (1980) with the slightly different value of 2.05.

At a small Reynolds number, on the other hand, we may use the estimate

$$\tau_{r\phi} \simeq \mu\frac{-\Omega a}{a} \tag{3.6}$$

to find

$$-L \simeq 8\pi\mu a^3\Omega, \tag{3.7}$$

where we have dropped a coefficient $1/3$ to conform with the exact Stokes-flow result (see e.g. Lamb 1932; Kim & Karrila 1991). In this regime, the flow disturbance decays sufficiently fast away from the sphere that a regular perturbation expansion in Re can be carried out. The first few terms were calculated by Bickley (1938) and Collins (1955) and are

$$-\frac{L}{8\pi\mu\Omega a^3} = 1 + \frac{Re^2}{1200} - \frac{15\,647}{20\,744\,640\,000}Re^4 + \cdots. \tag{3.8}$$

This series was extended by others and, notably, carried to terms of the order of Re^{20} by Shail (1997) by means of computer-algebra techniques.

Our numerical results for L versus Re are shown in figure 2 together with the asymptotic approximations (3.5) and (3.8). In this and in the following figures, symbols indicate the computed points. The agreement in the range of validity of the approximations is excellent and, in between, our results agree with those of Dennis *et al.* (1980), who showed that their simulations were in very good agreement with the experimental data of Sawatzki (1970).

It is intuitively evident that the centrifugal effect will produce a swirling radial jet directed outward of the equatorial region of the sphere, which must be maintained by a flow towards the poles in the direction of the axis of rotation. Figure 3 shows some pathlines for $Re = 1$ and $Re = 30$ which illustrate this phenomenon. The pitch of the particle trajectories increases significantly with Re.

The poleward flow will exert equal and opposite forces on each hemisphere so that the net force on the sphere vanishes. This cancellation will not occur, however, in the neighbourhood of a boundary where, therefore, the sphere will be subjected to a force as we show in the next section. In order to estimate this force, it is useful to consider the magnitude of the poleward velocity. Arguing from the equation of continuity, we may write

$$\frac{\partial w}{\partial z} \simeq \frac{w}{\sqrt{\nu/\Omega}} = -\frac{1}{r}\frac{\partial}{\partial r}(ru) \simeq \frac{\Omega a}{a}, \tag{3.9}$$

where w is the velocity along the rotation axis and u is the velocity in the radial direction. From this relation we find

$$\frac{w}{\Omega a} \sim Re^{-1/2}. \tag{3.10}$$

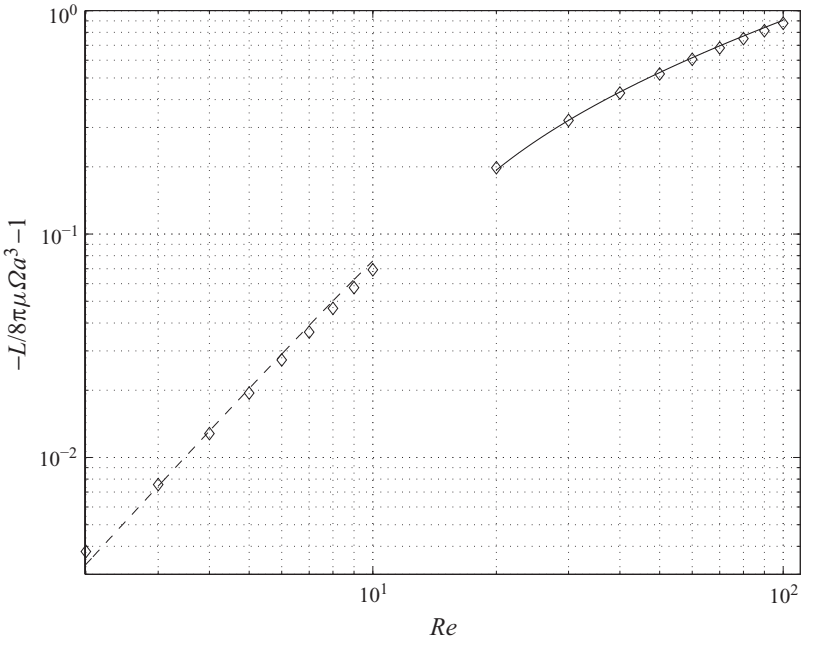

FIGURE 2. Hydrodynamic couple versus $Re = a^2\Omega/\nu$; the points are the present calculated values and the lines the large-Re asymptote (3.5) with the correction of Dennis *et al.* (1980), and the small-Re asymptote (3.8).

This is the same scaling as for the self-similar von Kármán's rotating disk flow (see e.g. Landau & Lifshitz 1987).

Unlike the von Kármán flow, in the present situation the velocity $|w|$ along the axis of rotation must go to zero far from the sphere and vanish at the poles. Thus, it must have an extremum point $|w|_{max}$ of which (3.10) represents the order of magnitude. Figure 4 shows a graph of $|w|_{max}/\Omega a$ versus Re on a log–log scale. After adjusting the constant by fitting the numerical results we find that the large-Re asymptote on the right is given by $(5Re^{-1/2})/9$. We will use this result in the next section to estimate the force on a sphere near a wall. The low-Re behaviour can be found simply by using a in place of $\sqrt{\nu/\Omega}$ to estimate the z-derivative in (3.9). After adjusting a constant as before, we find $|w|_{max}/(\Omega a) \simeq Re/75$.

3.2. *The transient problem*

For a vanishing Reynolds number, the transient problem is governed by the time-dependent Stokes equations which are readily solved with the result (Feuillebois & Lasek 1978; Gavze 1990)

$$-\frac{L}{8\pi\mu a^3} = \Omega(t) + \frac{1}{3}\Omega(0)\left[\frac{a}{\sqrt{\pi\nu t}} - \mathrm{e}^{\nu t/a^2}\,\mathrm{erfc}(\sqrt{\nu t}/a)\right] + \frac{1}{3}\int_{0+}^{t}\dot{\Omega}(\tau)\left[\frac{a}{\sqrt{\pi\nu(t-\tau)}} - \mathrm{e}^{\nu(t-\tau)/a^2}\,\mathrm{erfc}(\sqrt{\nu(t-\tau)}/a)\right]\mathrm{d}\tau, \quad (3.11)$$

where $\dot{\Omega} = \mathrm{d}\Omega/\mathrm{d}t$. Evidently the couple is infinite at $t = 0$ whenever $\Omega(0) \neq 0$, as could be expected. In particular, for an impulsively started constant rotation, $\dot{\Omega} = 0$

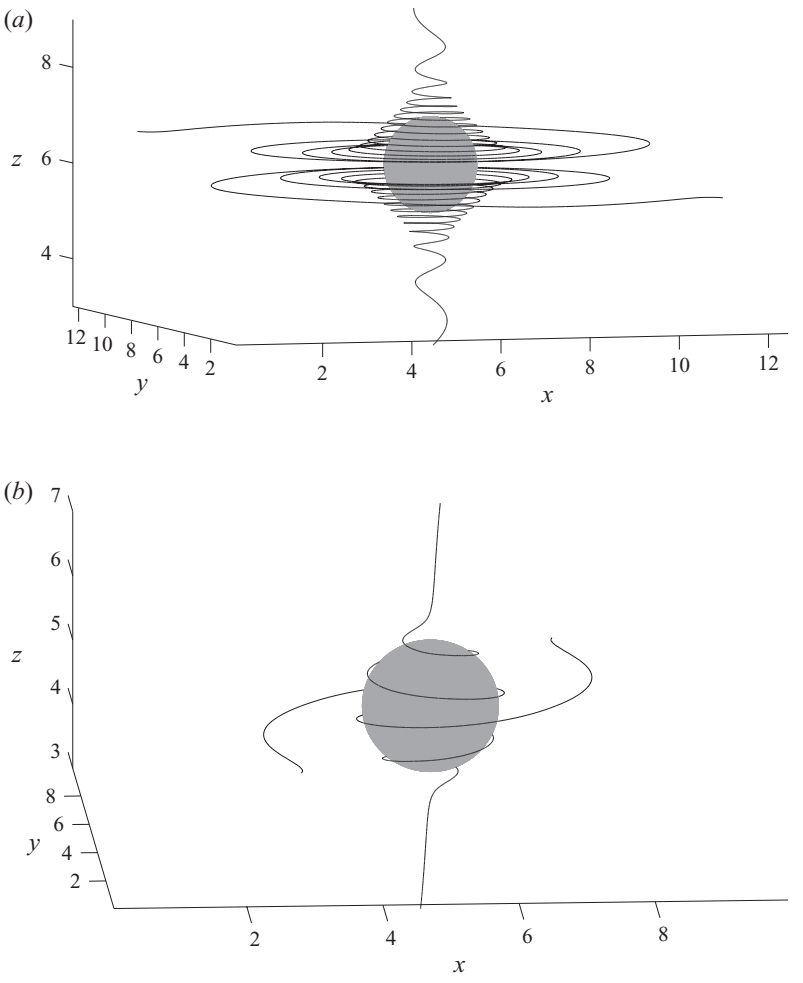

FIGURE 3. Some pathlines around a sphere rotating in an unbounded fluid at $Re = 1$ (a) and $Re = 30$ (b).

for $t \geqslant 0+$ and one finds

$$-\frac{L}{8\pi\mu a^3\Omega} = 1 + \frac{1}{3}\left[\frac{a}{\sqrt{\pi\nu t}} - \mathrm{e}^{\nu t/a^2}\,\mathrm{erfc}(\sqrt{\nu t}/a)\right]. \tag{3.12}$$

Up to a numerical constant, the leading-order term of this result can be found from (3.2) by using $\tau_{r\phi} \simeq \mu a\Omega/\sqrt{\nu t}$. As $t \to \infty$, (3.12) gives

$$-\frac{L}{8\pi\mu a^3\Omega} = 1 + \frac{\pi}{6}\left(\frac{a}{\sqrt{\pi\nu t}}\right)^3 + \cdots. \tag{3.13}$$

The transient effect is seen to decay much faster than that for the case of translation.

The time dependence of the hydrodynamic couple on an impulsively started sphere was calculated by Dennis & Duck (1988) for $Re = 1000$, 3000 and 5000. The trend of the results was the same in all cases, with a very large value for small times, a steep decline to a shallow minimum and a slight smooth rise to steady state. The

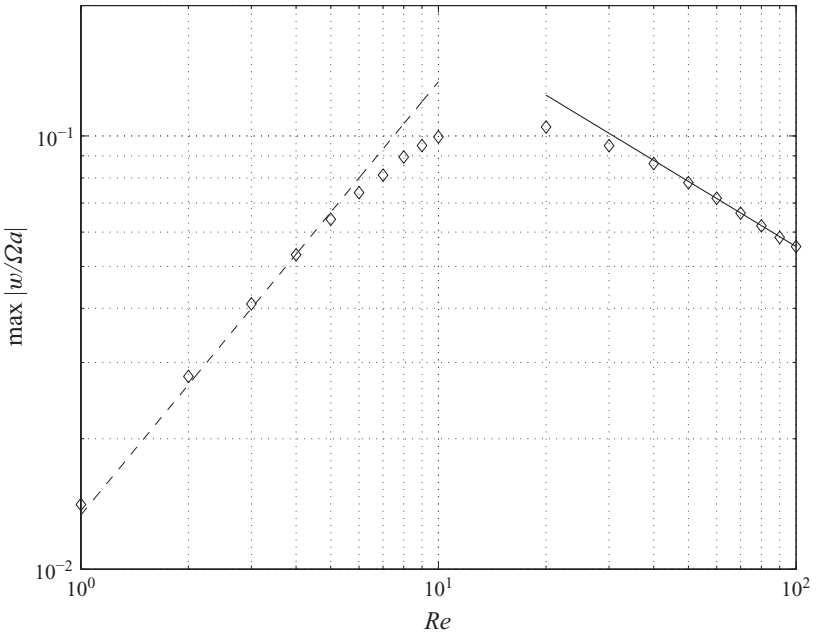

FIGURE 4. Maximum absolute velocity $|w/(\Omega a)|$ along the axis of a sphere rotating in an unbounded fluid as a function of the Reynolds number $a^2\Omega/\nu$. The two lines are fits proportional to Re and $Re^{-1/2}$, respectively, at small and large Reynolds numbers.

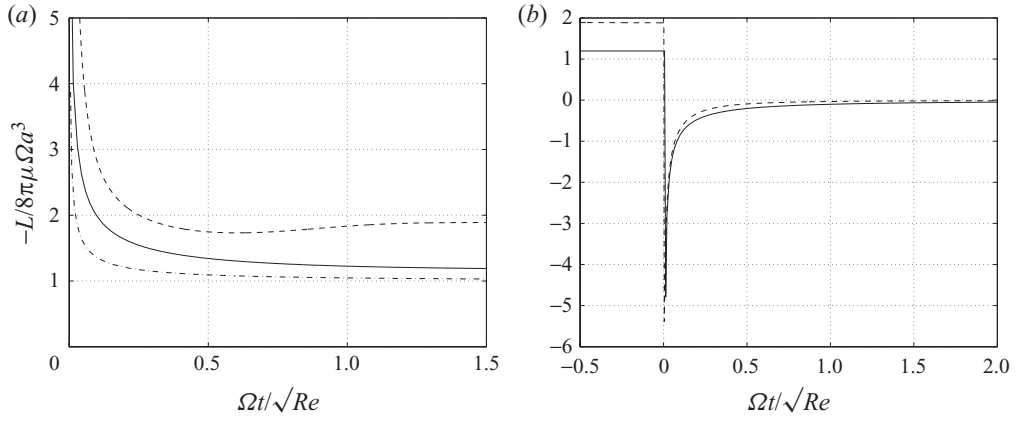

FIGURE 5. Transient hydrodynamic couple on an impulsively started (*a*) or stopped (*b*) sphere in an infinite fluid versus normalized time; in ascending order the lines are for $Re = 1$, $Re = 20$ and $Re = 100$; the $Re = 1$ line has been omitted in (*b*).

boundary-layer approximation gave very similar results except that the shallow minimum was not reproduced.

For the impulsively started sphere problem our method is inaccurate as long as the boundary layer is thinner than a few mesh lengths. However, by running simulations with different grids we have satisfied ourselves that this initial error becomes negligible at later times. Our results for $Re = 1$, 20 and 100 are plotted in figure 5 against $\Omega t/\sqrt{Re} = t\sqrt{\Omega\nu/a^2}$, namely time normalized by the geometric mean of the two time scales $1/\Omega$ and a^2/ν. For $Re = 1$ the couple decreases monotonically,

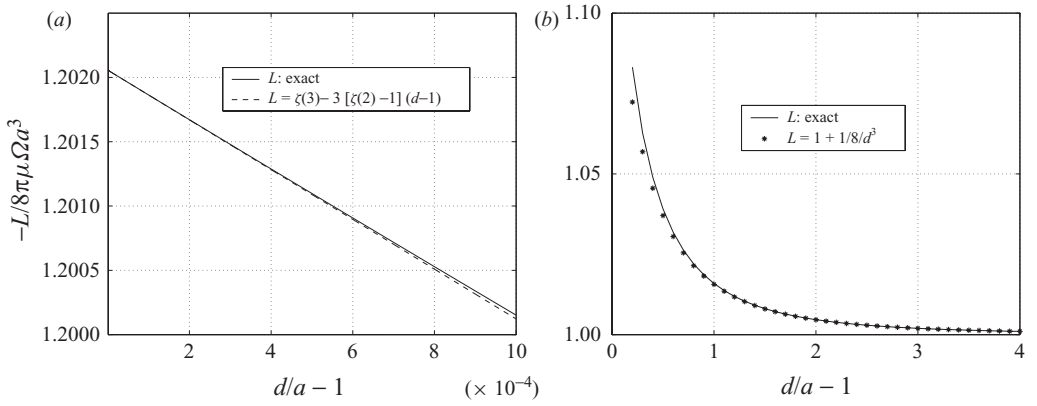

FIGURE 6. Comparison between the exact result for the hydrodynamic couple at $Re = 0$ (solid lines) and the near-wall approximation (4.1) (dashed line, a), and the leading-order result of the far-wall approximation (4.2) (asterisks, b).

while for $Re = 100$ the shallow minimum (followed by a very slight local maximum barely visible in the figure) is evident. The case with $Re = 20$ seems to be close to the threshold between a monotonic and non-monotonic decrease. The shallow minimum indicates that sufficient inertia causes a temporary thickening of the boundary layer before the radial jet can establish itself. Figure 5(b) shows corresponding results for an impulsively stopped sphere with $Re = 20$ and 100. The couple reaches very quickly a large positive value (probably not accurately calculated by our method for the reason explained before) and then decays monotonically to zero.

4. Rotation around an axis perpendicular to a plane boundary

In the Stokes limit, the problem of a sphere centred at a distance d from a plane boundary and rotating around an axis perpendicular to the plane (figure 1a) has been solved exactly by Jeffery (1915). The sphere rotates with a positive angular velocity around the x-axis.

From Jeffery's solution it can be shown that, when the sphere is very close to the plane,

$$-\frac{L}{8\pi\mu a^3\Omega} = \zeta(3) - 3\left(\frac{\pi^2}{6} - 1\right)\left(\frac{d}{a} - 1\right) + \cdots, \tag{4.1}$$

where ζ is Riemann's ζ-function and $\zeta(3) \simeq 1.20206$.

This result has been confirmed by a more direct method by Takagi (1974); the first term in the expansion was also given in Cox & Brenner (1967b). A remarkable feature of this result is that it remains finite as $d/a \to 1$. In the other limit of a sphere far from the plane one has (see also Brenner 1964)

$$-\frac{L}{8\pi\mu a^3\Omega} = \left[1 - \frac{1}{8}\left(\frac{a}{d}\right)^3 - \frac{3}{256}\left(\frac{a}{d}\right)^8 + \cdots\right]^{-1}. \tag{4.2}$$

The functional dependence predicted by (4.1) is compared with the exact result in figure 6(a); figure 6(b) is a comparison with the leading-order correction in (4.2).

Inertia introduces new and interesting features. The poleward flow on the wall side is retarded and unable to balance that coming from the opposite side with the result that the radial jet is now directed towards the plane (figure 7). This causes

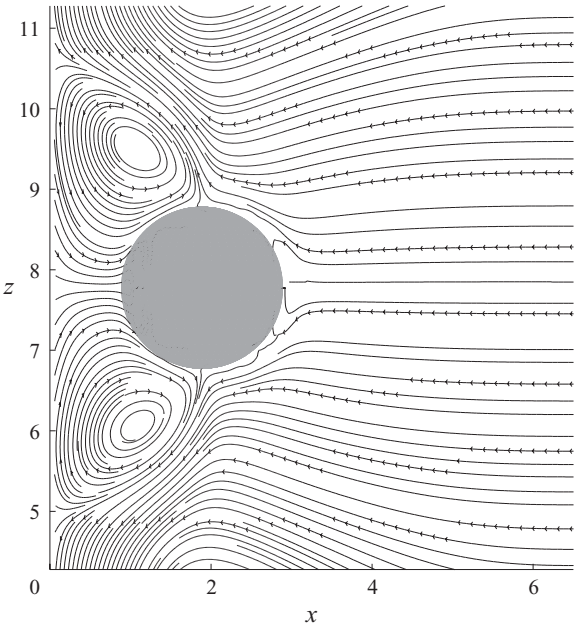

FIGURE 7. Sphere rotating around an axis perpendicular to a plane: traces of the stream surfaces in a plane containing the rotation axis for $Re = 100$ and $d/a = 17/9$. The plotting is somewhat under-resolved near the sphere surface.

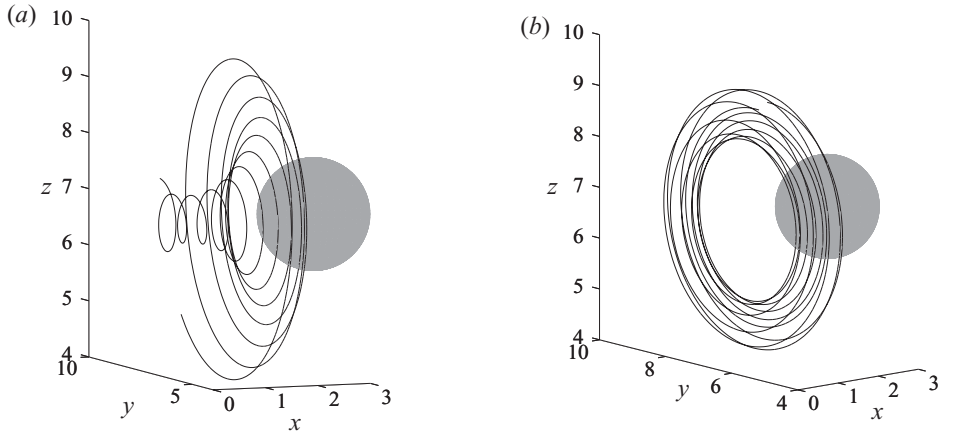

FIGURE 8. Two examples of the pathlines in the wall region for $Re = 1$ and $d/a = 3$. (*a*) The pathline starts near the wall, spirals up and outward towards the rotating sphere, and spirals back towards the wall. (*b*) The pathline resides on a toroidal surface.

a stagnation ring, with some of the fluid trapped between the radial jet and the plane. It can be seen from figure 7 that the pathlines of some of the fluid particles in this region reside on toroidal structures, while others have a more complex nature. Examples of these two behaviours are shown in figure 8 for $Re = 1$. This behaviour is less clear at higher Reynolds numbers as the spiralling motion is then faster as can be seen by comparing the two examples in figure 3.

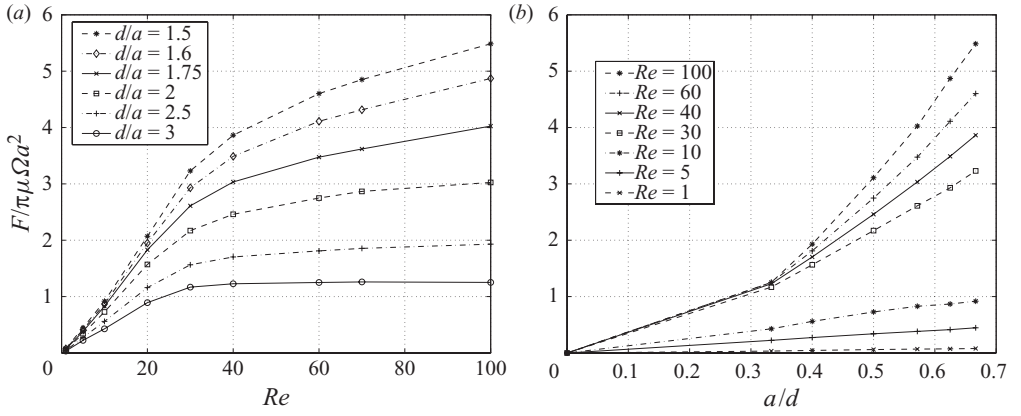

FIGURE 9. Dimensionless wall-directed force acting on a particle rotating around an axis perpendicular to the wall as a function of Re (a; lines in descending order with increasing d/a) and as a function of the inverse distance from the wall a/d (b; lines in ascending order with increasing Re).

The unbalanced fluid momentum in the direction of the axis causes the appearance of a force directed towards the plane. Another contribution to this force arises from the region of low pressure that forms between the sphere and the wall because of the rotational motion. Figure 9 shows the dimensionless force

$$\frac{F}{\pi\mu a^2\Omega} \tag{4.3}$$

versus Re for several values of d/a, and versus a/d for different Re. From the unbounded fluid case, the solution of the Navier–Stokes equations may be expected to be an analytic function of Re near $Re=0$. Thus, since F cannot depend on the direction of rotation, one expects $F=0$ at $Re=0$ and $F/\Omega \propto Re$ for small Re. The dependence can be non-analytic at large Re and, indeed, figure 9 suggests $F \propto |\Omega|$ for large Re. This behaviour can be understood recalling the estimate of the poleward velocity given earlier in (3.10). If we use the estimate $F \sim \pi a^2\rho w^2 \sim \pi a^2\rho(a^2\Omega^2 Re^{-1})$, we find $F/(\pi\mu a^2\Omega) \sim$ const. The value of the constant will depend on the extent to which the flow from the wall direction is impeded which, in its turn, depends on the distance from the wall. In general, one would expect the net force to decrease with distance away from the wall as indeed found numerically and shown in the figure. It is also seen that the asymptotic trend $F \propto \Omega$ is reached at higher and higher Reynolds numbers the closer the sphere is to the wall.

Figure 10 shows the hydrodynamic couple on the particle for various distances from the wall as a function of the Reynolds number. With respect to the infinite-fluid results of figure 2, in the smaller Reynolds number range the couple is increased by the wall-induced viscous dissipation. The results for $Re=1$ are seen to fall very close to the Stokes-flow solution denoted by asterisks in the figure. Viscosity becomes less significant at higher Re, when the flow feeding the equatorial jet becomes stronger and dominates the viscous stress on the sphere surface. This flow is impeded by the wall on one side of the sphere, which results in a lower viscous stress and a slightly smaller couple than in the case of an unbounded fluid over an intermediate range of wall–sphere distances.

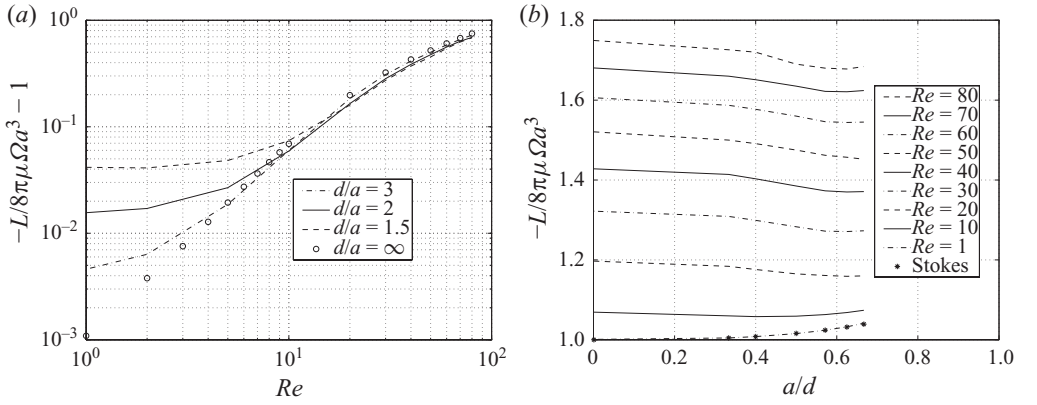

FIGURE 10. Hydrodynamic couple versus $Re = a^2\Omega/\nu$ at different distances from the wall (a) and versus the inverse distance from the wall a/d (b; lines in ascending order with increasing Re); the circles in (a) are the infinite-fluid results of figure 2.

5. Rotation around an axis parallel to a plane boundary

We now turn to the case in which the axis of rotation, which we take as the y-axis, is parallel to the wall (figure 1b). As before, the sphere rotates in the positive sense.

An approximate solution for the Stokes flow in this situation has been given by Goldman, Cox & Brenner (1967) and a more accurate one by Chaoui & Feuillebois (2003). When the sphere–wall gap is very small (Goldman *et al.* 1967) give

$$-\frac{L}{8\pi\mu a^3\Omega} \simeq \frac{2}{5}\log\frac{a}{d-a} + 0.3709 \tag{5.1}$$

while, in the opposite limit,

$$-\frac{L}{8\pi\mu a^3\Omega} \simeq 1 + \frac{5}{16}\left(\frac{a}{d}\right)^3. \tag{5.2}$$

The corresponding results for the force parallel to the wall are (Goldman *et al.* 1967)

$$-\frac{F_z}{\pi\mu a^2\Omega} = \frac{4}{5}\log\frac{a}{d-a} - 1.516 \tag{5.3}$$

and

$$-\frac{F_z}{\pi\mu a^2\Omega} = \frac{3}{4}\left(\frac{a}{d}\right)^4\left(1 - \frac{3}{8}\frac{a}{d}\right). \tag{5.4}$$

As in the previous case, inertia introduces some complexity in the flow as can be seen from the stream surfaces for $d/a = 3$ and $Re = 1$ and 50 shown in figures 11 and 12. At a low Reynolds number, the streamlines in the equatorial plane near the sphere weakly spiral outward (figure 11a) and, on a larger scale, viscosity produces a mainly downward flow parallel to the wall. At $Re = 50$ the radial jet is much stronger and causes a stagnation line on the solid wall (figure 12a). The wall pressure distribution for this case is portrayed in figure 13 and clearly shows the high pressure region in the neighbourhood of the stagnation line displaced away from the axis. Farther from the sphere the fluid tends to retain for a much greater distance the radial velocity component with which it is ejected from the sphere equator. In both

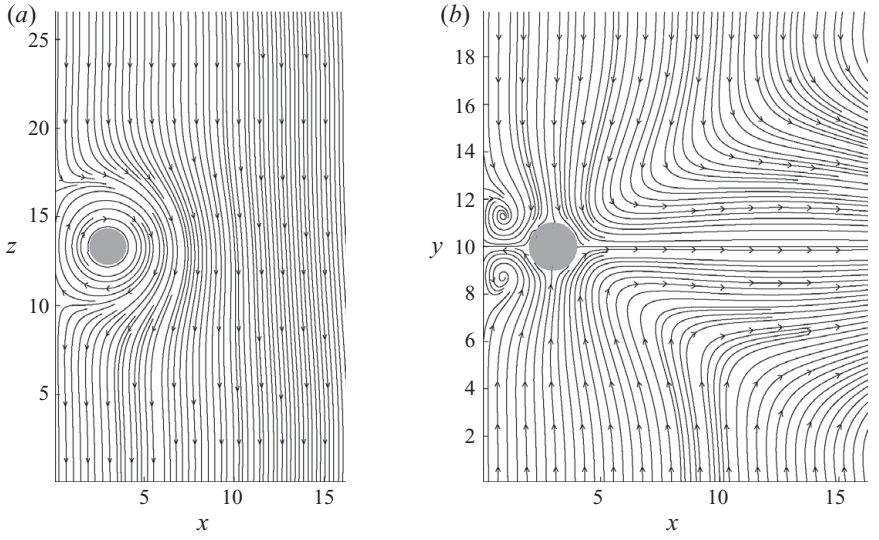

FIGURE 11. Stream surfaces for a sphere rotating near a wall around an axis parallel to the wall. (*a*) The trace of the stream surfaces in the equatorial plane of the sphere, which is rotating clockwise. (*b*) The trace of the stream surfaces on a plane perpendicular to the boundary and containing the axis of rotation; $Re = 1$, $d/a = 3$.

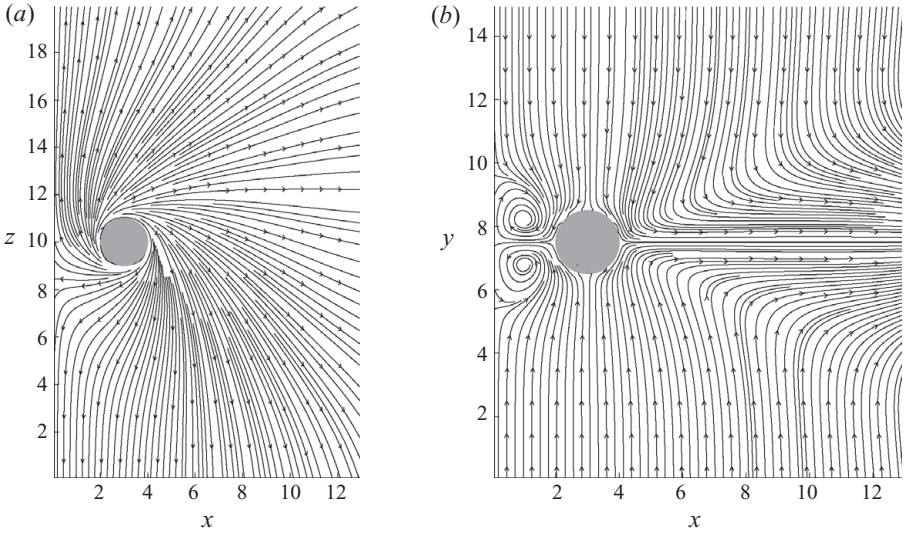

FIGURE 12. Stream surfaces for a sphere rotating near a wall around an axis parallel to the wall. (*a*) The trace of the stream surfaces in the equatorial plane of the sphere, which is rotating clockwise. (*b*) The trace of the stream surfaces on a plane perpendicular to the boundary and containing the axis of rotation; $Re = 50$, $d/a = 3$.

cases, in the plane normal to the wall and containing the axis of rotation, vortices form the magnitude of which increases with increasing Re (figures 11*b* and 12*b*).

The presence of the wall generates forces in the wall-normal and wall-parallel directions, F_x and F_z, respectively. These components, normalized as in (4.3), are shown in figures 14 and 15 as functions of Re and a/d. At the smaller Reynolds

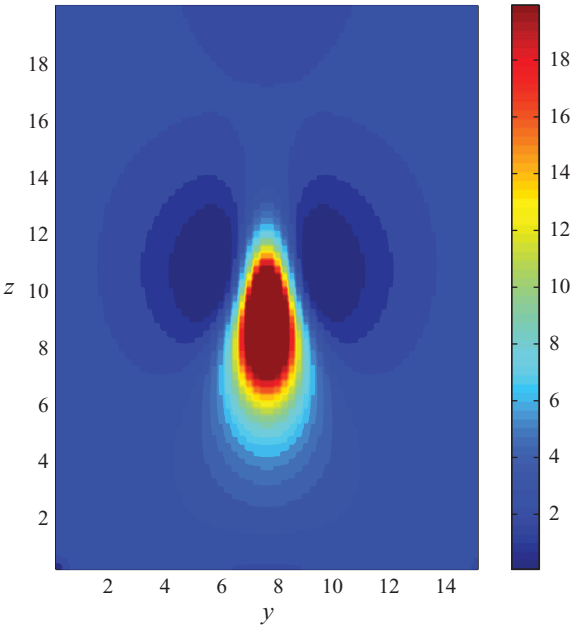

FIGURE 13. (Colour online) Wall pressure distribution on the solid wall generated by a sphere rotating around a horizontal axis parallel to the wall; $Re = 50$, $d/a = 3$. The sphere centre is at $y = 7.5$ and $z = 10$. The pressure maximum corresponds to the location where the radial wall-directed jet impinges the wall as shown in figure 12(*a*).

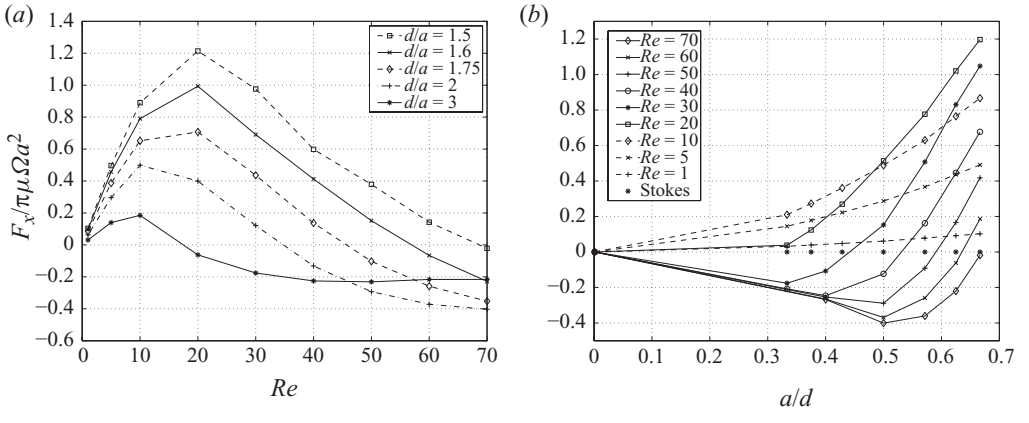

FIGURE 14. Dimensionless wall-normal force acting on a particle rotating around an axis parallel to the wall as a function of Re (*a*) and as a function of the inverse distance from the wall a/d (*b*). Positive and negative values of F_x denote forces directed away from and towards the wall, respectively.

number, viscous effects in the gap between the sphere and the wall dominate and the wall-normal force F_x is positive, i.e. repulsive, tending to push the particle away from the wall. As Re increases, F_x changes sign and becomes attractive. This latter behaviour is clearly a Bernoulli-type effect, similar to the potential-flow attraction by the wall of a sphere translating parallel to it (see e.g. Milne-Thomson 1968, § 17.61).

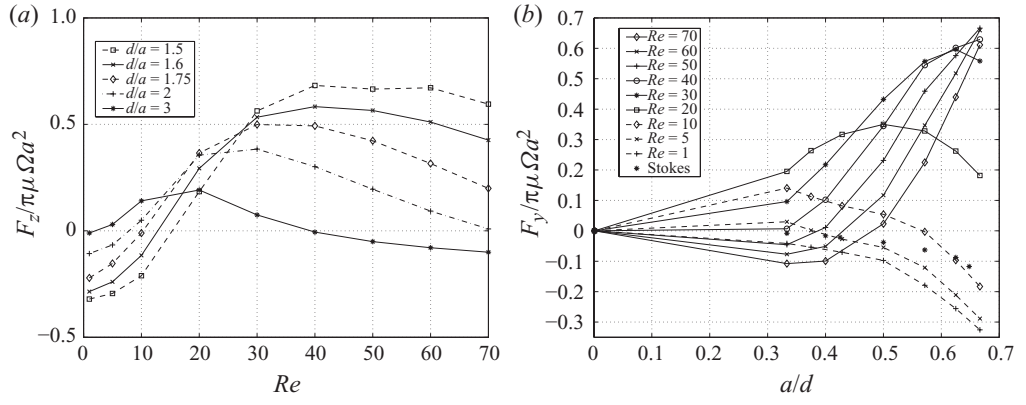

FIGURE 15. Dimensionless wall-parallel force acting on a particle rotating around an axis parallel to the wall as a function of Re (a) and as a function of the inverse distance from the wall a/d (b). Negative values denote a force oriented in the direction in which the sphere would roll down the plane if it were free.

The behaviour of the force component F_z parallel to the wall (figure 15) is more complex. When viscous effects are large, it is negative, i.e. in the direction in which the sphere would roll down the plane if it were free. This effect rapidly decreases as the distance from the wall increases and has essentially disappeared for $d/a = 3$. In an intermediate Reynolds number range the force becomes positive and then changes sign again. This behaviour may be understood with reference to the radial jet disturbed by the wall. At large Reynolds numbers the channeling imposed by the wall tends to direct this jet upward, with the consequence that the force on the sphere is downward by reaction. At intermediate Reynolds numbers, however, the adverse pressure gradient that develops along the wall above the sphere is strong enough to deflect this jet towards the wall normal, and the force is upward due to a combination of the high stagnation pressure and the downward momentum of the unimpeded part of the radial jet below the sphere.

It may be of some interest to note that plotting these results in the form

$$\frac{F_{x,z}}{\pi\mu a^2\Omega}\left(\frac{d}{a}-1\right) = f_{x,z}\left(Re\left(\frac{d}{a}-1\right)\right) \tag{5.5}$$

achieves an approximate collapse for both force components as long as d/a is not too large or Re not too small as shown in figure 16. The factor $Re(d/a-1)$ has the obvious meaning of a Reynolds number based on the gap between the sphere and the wall. The divergence of the force proportionally to $(d/a-1)^{-1}$ as $d/a \to 1$ is weaker than in the case of a rotating cylinder due to the curvature of the sphere in two directions rather than one only. This divergence is however stronger than logarithmic, which is the prediction of lubrication theory, as is easily verified, as well as of (5.3) for $Re = 0$.

Figure 17 shows the effect of the wall on the hydrodynamic couple on the sphere versus the inverse distance a/d from the wall. There is a relatively strong effect of the wall at the lower Reynolds numbers, for which the couple diverges when the sphere touches the wall as shown by (5.1). The results for $Re = 1$ are very close to those of the Stokes flow. At a higher Reynolds number, the couple is dominated by the shear stress associated with the two poleward flows found in the case of the sphere in an unbounded fluid. In this situation, unlike the case of the rotation

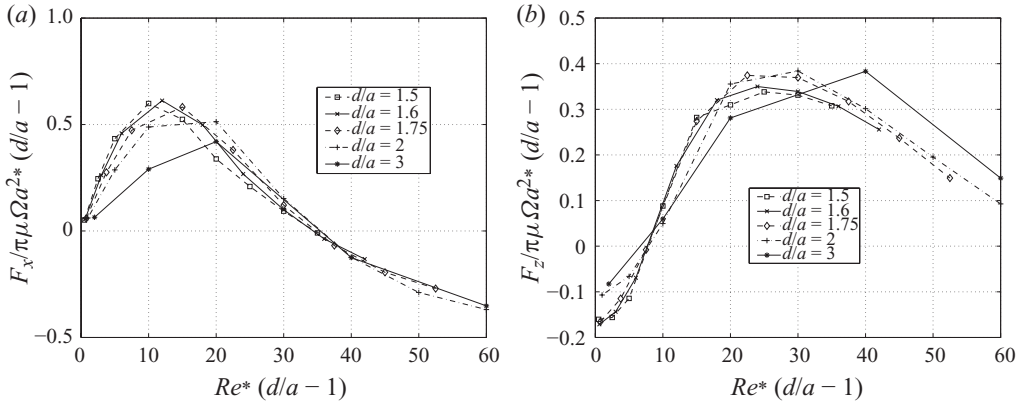

FIGURE 16. Wall-normal and wall-parallel forces for a sphere rotating about an axis parallel to a solid wall from figures 14 and 15 plotted in the scaled form suggested by (5.5).

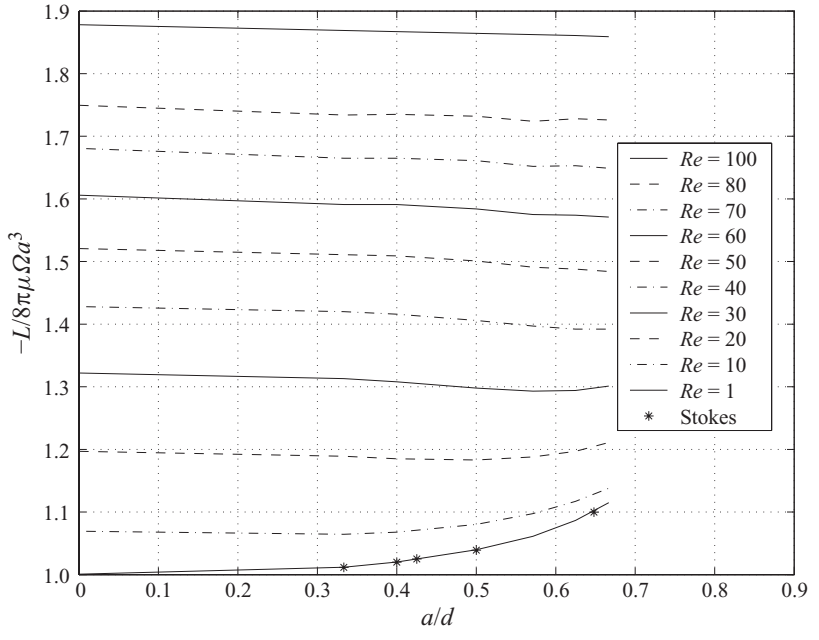

FIGURE 17. Hydrodynamic couple on a sphere rotating around an axis parallel to a solid wall. The horizontal axis is the inverse of the distance from the wall so as to permit a comparison with the case of an unbounded fluid of figure 2.

axis perpendicular to the wall, neither one of these flows is greatly affected by the wall and the resulting hydrodynamic couple is only very weakly dependent on a/d. Nevertheless, the presence of the wall prevents the radial jet from developing freely with a resulting accumulation of fluid in the gap between the sphere and the wall. This feature thickens the boundary layer and decreases somewhat the viscous stress on this portion of the sphere surface, which results in a shallow minimum of the couple before it finally rises to the value for an unbounded fluid. These same processes are encountered in the case of two walls and a cubic box discussed in the next two sections, but their importance is then enhanced.

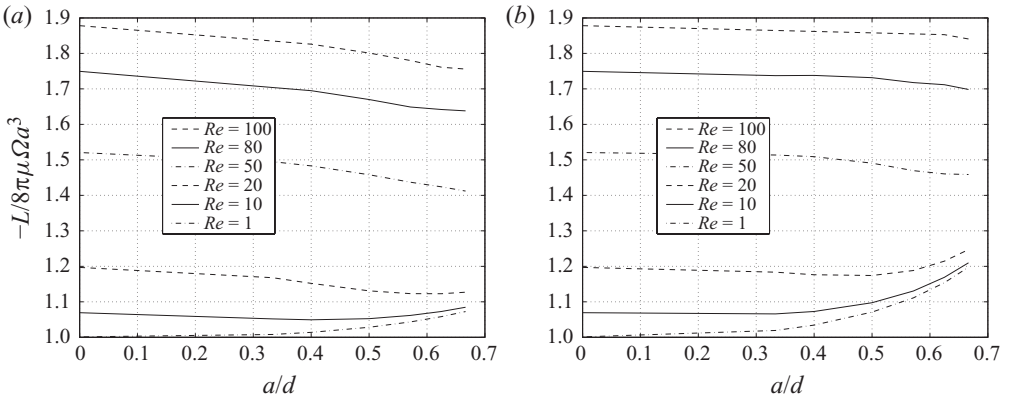

FIGURE 18. Hydrodynamic couple on a sphere rotating between two parallel walls around an axis perpendicular (a) and parallel to the walls (b). The horizontal axis is the inverse of the distance from the wall so as to permit a comparison with the case of an unbounded fluid of figure 2.

6. Sphere between two planes

We now study the effects of adding a second plane parallel to the first one and symmetrically placed with respect to the sphere (figure 1c,d). Because of symmetry there is a couple but no net force on the sphere.

Figure 18(a) is for a wall-perpendicular axis of rotation, which we take to be the x-axis. When the gap is small, viscous effects are large and so is the couple. As the gap widens, viscous effects decrease and, at sufficiently large Reynolds numbers, the couple becomes more and more affected by the poleward flow. For intermediate distances this flow is impeded by the walls but, eventually, it can proceed with little obstruction and the couple approaches the infinite-fluid result. These different physical mechanisms produce a couple which, when the Reynolds number is large enough, has a shallow minimum at an intermediate gap width. Qualitatively, this is the same behaviour observed in the case of a single wall in figure 10 although the effect is reinforced by the presence of the second wall.

Qualitatively, the couple for the case in which the axis of rotation is parallel to the walls (figure 18b) is very similar to that of a single wall shown in figure 17. The same physical mechanisms are at work, but with a somewhat greater intensity.

7. Sphere enclosed in a cube

The last case we consider is that of a sphere enclosed in a concentric cubic box of side $2d$; the axis of rotation is perpendicular to a pair of opposing faces of the cube.

For the couple, the correction to the Stokes-flow, infinite-fluid result (3.7) remains nearly constant over a significant range of Reynolds numbers which increases as the box size decreases as shown by figure 19(a). For fixed Re, the general trend of the couple as a function of a/d, the ratio of the sphere radius to the box side, shown in figure 19(b) is qualitatively similar to what is observed for two walls in figure 18 and one wall in figure 17. The physical mechanisms discussed in those cases are relevant for the present one as well and explain the observed features of the results.

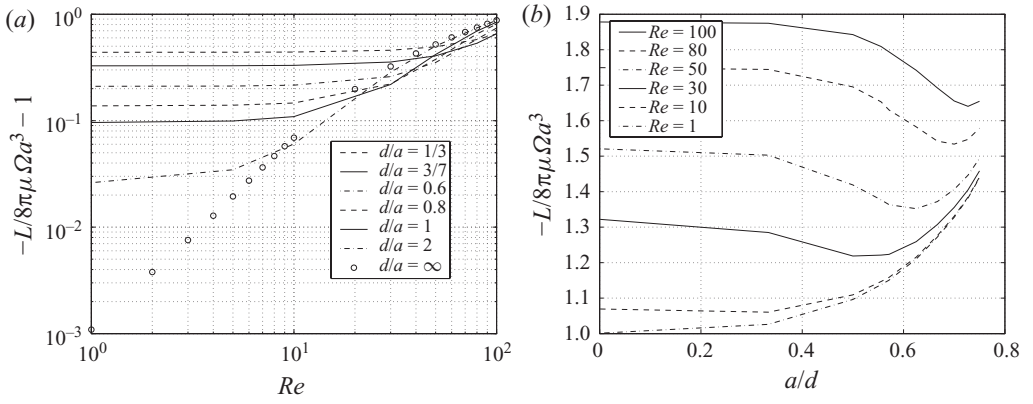

FIGURE 19. Hydrodynamic couple on a sphere rotating inside a cube of side $2d$.

8. Summary

In this paper we have studied several effects of neighbouring boundaries on the steady flow induced by a rotating sphere. When the boundaries destroy the symmetry about the sphere equator, forces develop which may be directed towards or away from the boundary and parallel or anti-parallel to it depending on the rotational Reynolds number $a^2\Omega/\nu$ and the distance from the wall. These forces would affect, for example, the deposition of particles: a particle rotating as the result of the interaction with a turbulent eddy might be repelled or attracted by a neighbouring wall as it moves towards it.

Though simple, the flows we have studied exhibit an interesting and perhaps unexpected richness under the action of the competing action of centrifugal, inertial and viscous effects. The meridional pressure gradient induced by the centrifugal force drives fluid from the poles towards the equator, from which it moves outward in the form of a radial jet. Boundaries which break the axial symmetry of this jet induce reaction forces. Small Reynolds numbers and sphere–wall gap widths bring into play strong viscous effects which cause repulsive forces. Larger Reynolds numbers cause a Bernoulli effect in the gap, which may turn the forces into attractive ones.

This work has been supported by NSF grants CBET 0625138 and CBET 0754344.

REFERENCES

BANKS, W. H. H. 1976 The laminar boundary layer on a rotating sphere. *Acta Mech.* **24**, 273–287.

BARRETT, K. E. 1967 On the impulsively started rotating sphere. *J. Fluid Mech.* **27**, 779–788.

BESSERIS, G. J., MILLER, I. F. & YEATES, D. B. 1999 Rotational magnetic particle microrheometry: the Newtonian case. *J. Rheol.* **43**, 591–608.

BICKLEY, W. G. 1938 The secondary flow due to a sphere rotating in a viscous fluid. *Phil. Mag.* **25**, 746–752.

BRENNER, H. 1964 Slow viscous rotation of an axisymmetric body within a circular cylinder of finite length. *Appl. Sci. Res.* A **13**, 81–120.

BUSH, J. W. M., STONE, H. A. & TANZOSH, J. P. 1994 Particle motion in rotating viscous fluids: historical survey and recent developments. *Curr. Top. Phys. Fluids* **1**, 337–355.

CHAOUI, M. & FEUILLEBOIS, F. 2003 Creeping flow around a small sphere in a shear flow close to a wall. *Q. J. Mech. Appl. Nath.* **56**, 381–410.

COLLINS, W. D. 1955 On the steady rotation of a sphere in a viscous fluid. *Mathematika* **2**, 42–47.

Cox, R. G. & Brenner, H. 1967*a* Effect of boundaries on the Stokes resistance of an arbitrary particle. Part 3. Translation and rotation. *J. Fluid Mech.* **28**, 391–411.

Cox, R. G. & Brenner, H. 1967*b* The slow motion of a sphere through a viscous fluid towards a plane surface. II. Small gap widths, including inertial effects. *Chem. Engng Sci.* **22**, 1753–1777.

Damiano, E. R., Long, D. S., El-Khatib, F. H. & Stace, T. M. 2004 On the motion of a sphere in a Stokes flow parallel to a Brinkman medium. *J. Fluid Mech.* **500**, 75–101.

Dean, W. R. & O'Neill, M. E. 1963 A slow rotation of viscous liquid caused by the rotation of a solid sphere. *Mathematika* **10**, 13–24.

Dennis, S. C. R. & Duck, P. W. 1988 Unsteady flow due to an impulsively started rotating sphere. *Comput. Fluids* **16**, 291–310.

Dennis, S. C. R., Ingham, D. B. & Singh, S. N. 1981 The steady flow of a viscous fluid due to a rotating sphere. *Q. J. Mech. Appl. Math.* **34**, 361–381.

Dennis, S. C. R., Singh, S. N. & Ingham, D. B. 1980 The steady flow due to a rotating sphere at low and moderate Reynolds numbers. *J. Fluid Mech.* **101**, 257–279.

Feuillebois, F. & Lasek, A. 1978 On the rotational historic term in non-stationary Stokes flow. *Q. J. Mech. Appl. Math.* **31**, 435–443.

Fletcher, C. 1988 *Computational Techniques for Fluid Dynamics*. Springer.

Ganatos, P., Pfeffer, R. & Weinbaum, S. 1980*a* Strong interaction theory for the creeping motion of a sphere between plane parallel boundaries. Part 2. Parallel motion. *J. Fluid Mech.* **99**, 755–783.

Ganatos, P., Weinbaum, S. & Pfeffer, R. 1980*b* Strong interaction theory for the creeping motion of a sphere between plane parallel boundaries. Part 1. Perpendicular motion. *J. Fluid Mech.* **99**, 739–754.

Garrett, S. J. & Peake, N. 2002 The stability of the boundary layer on a rotating sphere. *J. Fluid Mech.* **456**, 199–218.

Gavze, E. 1990 The accelerated motion of rigid bodies in non-steady Stokes flow. *Intl J. Multiphase Flow* **16**, 153–166.

Goldman, A. J., Cox, R. G. & Brenner, H. 1967 Slow viscous motion of a sphere parallel to a plane wall. Part I. Motion through a quiescent fluid. *Chem. Engng Sci.* **22**, 637–651.

Happel, J. & Brenner, H. 1973 *Low-Reynolds Number Hydrodynamics, with Special Applications to Particulate Media*, 2nd edn. Noordhoff.

Hollerbach, R., Wiener, R. J., Sullivan, I. S., Donnelly, R. J. & Barenghi, C. F. 2002 The flow around a torsionally oscillating sphere. *Phys. Fluids* **14**, 4192–4205.

Jeffery, G. B. 1915 On the steady rotation of a solid of revolution in a viscous fluid. *Proc. Lond. Math. Soc.* **14**, 327–338.

Keh, H. J. & Chen, P. Y. 2001 Slow motion of a droplet between two parallel plane walls. *Chem. Engng Sci.* **56**, 6863–6871.

Kim, S. & Karrila, S. 1991 *Microhydrodynamics*. Butterworth (reprinted by Dover 2005).

Kohama, Y. & Kobayashi, R. 1983 Boundary-layer transition and the behaviour of spiral vortices on rotating spheres. *J. Fluid Mech.* **137**, 153–164.

Lamb, H. 1932 *Hydrodynamics*, 6th edn. Cambridge University Press.

Landau, L. & Lifshitz, E. 1987 *Fluid Mechanics*, 2nd edn. Pergamon.

Leach, J., Mushfique, H., Keen, S., Di Leonardo, R., Ruocco, G., Cooper, J. M. & Padgett, M. 2009 Comparison of Faxn's correction for a microsphere translating or rotating near a surface. *Phys. Rev.* E **79**, 026301.

Loper, D. E. 2001 On the structure of a Taylor column driven by a buoyant parcel in an unbounded rotating fluid. *J. Fluid Mech.* **427**, 131–165.

Malysa, K. & van de Ven, T. G. M. 1986 Rotational and translational motion of a sphere parallel to a wall. *Intl J. Multiphase Flow* **12**, 459–468.

Milne-Thomson, L. 1968 *Theoretical Hydrodynamics*, 5th edn. MacMillan.

Minkov, E., Ungarish, M. & Israeli, M. 2000 The motion generated by a rising particle in a rotating fluid – numerical solutions. Part 1. A short container. *J. Fluid Mech.* **413**, 111–148.

Minkov, E., Ungarish, M. & Israeli, M. 2002 The motion generated by a rising particle in a rotating fluid – numerical solutions. Part 2. The long container case. *J. Fluid Mech.* **454**, 345–364.

O'Neill, M. E. 1964 A slow motion of viscous liquid caused by a slowly moving solid sphere. *Mathematika* **11**, 67–74.

Parkin, S. J. W., Knner, G., Nieminen, T. A., Heckenberg, N. R. & Rubinsztein-Dunlop, H. 2007 Microrheology of microlitre samples: probed with rotating optical tweezers. *Proc. SPIE* **6644**, 66440O.

Peyret, R. & Taylor, T. 1983 *Computational Methods for Fluid Flow*. Springer.

Sawatzki, O. 1970 Das strömungsfeld um eine rotierende kugel. *Acta Mech.* **9**, 159–214.

Shail, R. 1997 Some regular perturbation solutions in fluid mechanics. *Q. J. Mech. Appl. Math.* **50**, 128–147.

Takagi, H. 1974 Slow rotation of two touching spheres in viscous fluid. *J. Phys. Soc. Japan* **36**, 875–877.

Taniguchi, H., Kobayashi, T. & Fukunishi, Y. 1998 Stability of the boundary layer on a sphere rotating in still fluid. *Acta Mech.* **129**, 243–253.

Walters, K. & Waters, N. D. 1963 On the use of a rotating sphere in the measurement of elasto-viscous parameters. *Brit. J. Appl. Phys.* **14**, 667–671.

Walters, K. & Waters, N. D. 1964 The interpretation of experimental results obtained from a rotating-sphere elasto-viscometer. *Brit. J. Appl. Phys.* **15**, 989–991.

Wimmer, M. 1988 Viscous flows and instabilities near rotating bodies. *Prog. Aerospace Sci.* **25**, 43–103.

Wu, X., Cen, K., Luo, Z., Wang, Q. & Fang, M. 2008*a* Measurement on particle rotation speed in gas–solid flow based on identification of particle rotation axis. *Exp. Fluids* **45**, 1117–1128.

Wu, X., Wang, Q., Luo, Z., Fang, M. & Cen, K. 2008*b* Theoretical and experimental investigations on particle rotation speed in a CFB riser. *Chem. Engng Sci.* **63**, 3979–3987.

Xin, J. & Megaridis, C. 1996 Droplet spindown in a high-temperature gas environment. *Intl J. Heat Fluid Flow* **17**, 567–578.

Zhang, Z. Z. & Prosperetti, A. 2005 Sedimentation of 1.024 particles. In *Proceedings of the ASME Fluids Engineering Division Summer Conference*, Paper no. FEDSM2005–77133. ASME.